# In situ high-potential-driven surface restructuring of ternary AgPd–Pt$_{dilute}$ aerogels with record-high performance improvement for formate oxidation electrocatalysis

Wang, Jiali; Chen, Fuyi; Jin, Yachao; Guo, Longfei; Gong, Xiaofang; Wang, Xiaolu; Johnston, Roy L.

*DOI:*
10.1039/C9NR03266E

Nanoscale

Accepted Manuscript

This article can be cited before page numbers have been issued, to do this please use: J. Wang, F. Chen, Y. Jin, L. Guo, X. Gong, X. Wang and R. L. Johnston, *Nanoscale*, 2019, DOI: 10.1039/C9NR03266E.

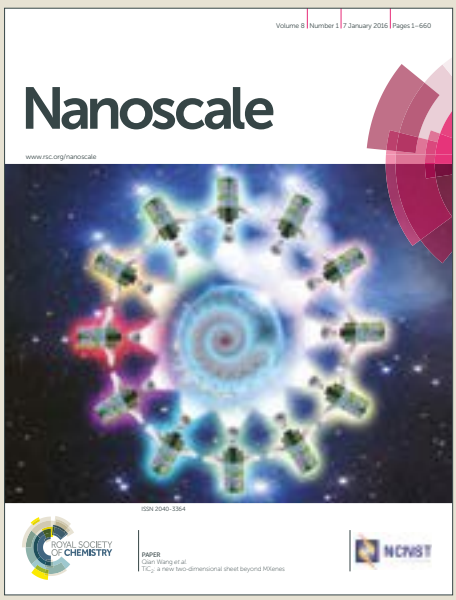




ROYAL SOCIETY OF CHEMISTRY

rsc.li/nanoscale

View Article Online
DOI: 10.1039/C9NR03266E

ARTICLE

# *In-situ* High-Potential-Driven Surface Restructuring of Ternary AgPd-Pt$_{dilute}$ Aerogels with Record High Performance Improvement for Formate Oxidation Electrocatalysis†

Received 00th January 20xx,
Accepted 00th January 20xx

DOI: 10.1039/x0xx00000x

Jiali Wang,[a,b] Fuyi Chen,*[a,b] Yachao Jin,[a,b] Longfei Guo,[a,b] Xiaofang Gong,[a,b] Xiaolu Wang,[a,b] and Roy L. Johnston [c]

Engineering nanoparticle surface driven by various gas atmospheres has attracted intensive attention to design efficient electrocatalysts for sustainable energy applications, however, developing a more facile and efficient *in-situ* engineering strategy under electrochemical testing conditions to achieve surface-reconstruction-induced high performance significantly lacks. Herein, for the first time, we report an *in-situ* high-potential-driven restructuring in ternary AgPdPt aerogels with dilute Pt (AgPd-Pt$_{dilute}$) during the electrochemical cyclic voltammetry testing for alkaline formate oxidation reaction (FOR), in which the upper potential limit is ingeniously enlarged to the Ag redox region. Impressively, the resulted AgPd-Pt$_{dilute}$ aerogel displays remarkably structural and compositional reconstruction in alkaline environment. Our comprehensive results reveal that the high-potential cycling induces the unique Ag outward diffusion to form enriched PdPt metallic surface atomically coupled with amorphous $Ag_2O$, which provides more opportunities to expose abundant active sites and induce the robust electronic structure modulation. Notably, the surface-restructured AgPd-Pt$_{dilute}$ aerogel achieves the record-high activity for FOR when the upper potential limit is enlarged to 1.3 V, exhibiting an unprecedented 5-fold activity improvement compared to the commercial Pd/C. Moreover, it also offers greatly enhanced electrochemical stability with the negligible activity decay after 500 cycles. This work gives a good understanding of surface reconstruction during such a novel high-potential-driven cycling process and opens a new door to design more efficient electrocatalysts for FOR and beyond.

## Introduction

Direct formate fuel cells (DFFCs) are attracting extensive attention as dominant energy conversion devices due to the relatively high power density and theoretical potential among different kinds of direct liquid alkaline membrane fuel cells.[1-6] Moreover, the fuel formate salts can be easily derived from the reduction of carbon dioxide at high Faradaic efficiencies and then be safely stored and transported in their solid state, making the DFFCs not only be the promising alternative to the existing hydrogen-based fuel cells but also facilitate to achieve carbon-neutral energy consumption.[7-10] However, the broad deployment and widespread commercialization of DFFCs are impeded by the lack of a highly active and stable electrocatalyst for the anode formate oxidation reaction (FOR) in alkaline media.[6, 11] Currently, Pd has been regarded as the state-of-the-art electrocatalyst for FOR because of its high catalytic activity and anti-CO poisoning stability.[4-6] The oxidation of formate on Pd dominantly proceeds via the dehydrogenation to $CO_2$ ($HCOO^-_{ad} \rightarrow H_{ad} + COO^-_{ad}$, $H_{ad} + OH^- \rightarrow H_2O + e^-$, $COO^-_{ad} \rightarrow CO_2 + e^-$), but the strong bonding of adsorbed hydrogen ($H_{ad}$) intermediates on pure Pd leads to its still unsatisfactory FOR activity.[4, 12] To improve the electrocatalytic performance of Pd for FOR, the primarily sought strategy is the rational design of multicomponent Pd-based alloys.[5, 13] For example, Noborikawa et al. synthesized PdCu nanoparticles supported on the activated carbon for FOR, which shows a 1.77-fold activity improvement compared with the commercial Pd/C.[14] Sankar et al. recently have prepared a series of PdCo/C electrocatalysts for FOR, and the peak current density of the best $Pd_{2.3}Co$/C is 1.72 times higher than that of Pd/C.[15] Despite tremendous efforts over the past decades,[14-16] these reported Pd-based alloy electrocatalysts only achieve small performance gains for FOR. The conventional alloying strategy on Pd for the further activity improvement of FOR is extremely limited for the practical operation of DFFCs considering that at least a 3 to 5-fold remarkable enhancement can be achieved by using alloyed electrocatalysts in hydrogen fuel cells.[9, 17, 18] To the best of our knowledge, there are few, if any, existing examples of FOR electrocatalysts that could be twice better in electrocatalytic activity than the commercial Pd/C.

Surface engineering of nanoparticles surface, as a promising alternative strategy for size or shape controlling to achieve high catalytic performance, is becoming one of the most efficient

[a] State Key Laboratory of Solidification Processing, Northwestern Polytechnical University, Xi'an, 710072, China. E-mail: fuyichen@nwpu.edu.cn
[b] School of Materials Science and Engineering, Northwestern Polytechnical University, Xi'an, 710072, China.
[c] School of Chemistry, University of Birmingham, B15 2TT, UK.
†Electronic Supplementary Information (ESI) available: Additional SEM and TEM images, XRD patterns, electrocatalytic FOR performances. See DOI: 10.1039/x0xx00000x

View Article Online
DOI: 10.1039/C9NR03264F

approaches to design advanced electrocatalysts for various reactions.[19-22] Especially, the surface engineering process driven by the specific gas atmosphere has been widely reported to endow pristine electrocatalysts with remarkable reconstruction and enhanced catalytic properties. Zhao et al. employed the annealing process under oxygen atmosphere to introduce the NiO-enriched surface in Pt-Ni bimetallic nanoparticles, which delivers the highest activity for hydrogen evolution reaction in alkaline media.[21] Very recently, Shen et al. report the surface segregation and oxidation of Ni and Cu atoms in ternary Pt-Cu-Ni nanoparticles in an oxidative environment at elevated temperatures, which establishes a volcano relationship between the oxygen reduction reaction activity and segregation extents through adjusting the duration time of air annealing, achieving much higher catalytic activity than that of pristine electrocatalysts.[22] It is believed that the synergetic effects between active metals and oxidized species originating from restructuring process play a critical role in greatly promoting electrocatalytic reactions. Although gas atmosphere induced surface restructuring exhibits its excellent capacity to engineer catalyst for enhanced electrocatalytic performance, it should be noted that there are still several challenges need to be paid more attention. Firstly, the gas-induced surface restructuring strategy depends heavily on the annealing process with well-designed gas atmospheres, temperatures and time schedules, which is really complex and greatly increases the overall cost of catalysts preparation. Secondly, the significant surface metal derivatives such as oxides induced by the atmosphere annealing treatment are reported to be dominated with usual crystalline nanostructures. It has been recently found that the amorphous phases have more prominent effect on catalytic properties compared with their crystalline counterparts.[23, 24] Inspired by the aforementioned discussions, it is highly attractive to explore a more facile and efficient engineering strategy to incorporate favorable structural and compositional features into Pd-based electrocatalyst to achieve exceptional FOR activity.

Herein, we for the first time develop an *in-situ* high-potential-driven restructuring strategy during the electrochemical testing to engineering trimetallic AgPdPt aerogels with dilute Pt (denoted as AgPd-Pt$_{dilute}$ hereafter) as a new class of high-performance electrocatalyst for FOR in alkaline media. When the upper potential limit is judiciously enlarged from the conventional value of 1.1 V to the Ag redox region of 1.3 V, a surface-restructured AgPd-Pt$_{dilute}$-1.3 aerogel was achieved. Systematically physical and electrochemical characterizations reveal the unique Ag element outward diffusion under high-potential cycling, which induces the enriched PdPt surface atomically coupled with $Ag_2O$ domains with amorphous nature. Benefiting from the much more exposed active sites and effectively modified electronic band structure originating from strong interactions between amorphous Ag oxide with catalytic metals, the surface-restructured AgPd-Pt$_{dilute}$-1.3 aerogel exhibits the unprecedented electrocatalytic activity and stability improvement for FOR, representing the best performance among all the FOR electrocatalysts reported to date. Significantly, the record-high catalytic performance offered by our surface-restructured AgPd-Pt$_{dilute}$-1.3 aerogel highlights the important role of Ag redox process over other metals for the great catalytic activity improvement, which provides more insights into designing more excellent electrocatalysts for future energy conversion and storage devices. So far, very few studies are focusing on the *in situ* high-potential-driven structural and compositional restructuring of ternary electrocatalysts during the electrochemical reactions, which is crucial to their remarkably enhanced catalytic performance.

## Experimental Section

### Synthesis of bimetallic AgPd aerogels

The AgPd hydrogels were efficiently synthesized by an accelerated kinetically controlled strategy in aqueous solution. In a typical synthesis of $Ag_1Pd_2$ hydrogel, 8 mL of 10 mM $H_2PdCl_4$ and 4 mL of 10 mM $AgNO_3$ (the final total concentration 0.3 mM) were successively dropped in 383.5 mL ultrapure water and stirred for 10 min at 60 °C, then 4.5 mL of freshly prepared 60 mM $NaBH_4$ aqueous solution was quickly added dropwise. The slight yellow solution gradually changed to black. The solution was kept stirring for three minutes and then allowed to settle still at 60 °C. After 4 hours, a thin layer of $Ag_1Pd_2$ hydrogel was formed at the bottom of the beaker and the solution became colorless. The obtained $Ag_1Pd_2$ hydrogel was washed with three cycles of NaCl saturated water solution and three cycles of water to dissolve the silver chloride formed in the production process (Fig. S1, Supporting Information). After carefully washing, $Ag_1Pd_2$ aerogel was obtained from freeze-dried process overnight. Other $Ag_xPd_y$ aerogels with different Ag/Pd atomic ratios (x:y = 1:3, 1:1 and 2:1) were also prepared by simply changing the mole ratios of Ag and Pd precursors but making the total concentration unchanged (Table S1, Supporting Information).

### Synthesis of trimetallic AgPd-Pt$_{dilute}$ aerogels

In a typical synthesis of $Ag_1Pd_2$-$Pt_{0.25}$ hydrogel, 0.92 mL of 10 mM $H_2PtCl_6$, 7.4 mL of 10 mM $H_2PdCl_4$ and 3.68 mL of 10 mM $AgNO_3$ (the final total concentration 0.3 mM) were successively dropped in 383.5 mL $H_2O$ and stirred for 10 min at 60 °C, then 4.5 mL of freshly prepared 60 mM $NaBH_4$ aqueous solution was quickly added dropwise. The solution was kept stirring for three minutes and then allowed to settle still at 60 °C. After 4 hours, the $Ag_1Pd_2$-$Pt_{0.25}$ hydrogel was formed at the bottom of the beaker. The dissolution of silver chloride was achieved via a similar procedure mentioned above. After that, $Ag_1Pd_2$-$Pt_{0.25}$ aerogel was obtained from freeze-dried process. In addition, other $Ag_xPd_y$-Pt aerogels with various Ag/Pd atomic ratios (x:y = 1:3, 1:1 and 2:1) and the same dilute Pt content were also synthesized (Table S1, Supporting Information). For clarity, we use AgPd and AgPd-Pt$_{dilute}$ in this work represents the as-synthesized $Ag_1Pd_2$ and $Ag_1Pd_2$-$Pt_{0.25}$ aerogels, respectively, unless otherwise stated.

### Physical characterizations

Transmission electron microscopy (TEM) images were obtained on a FEI Talos F200X TEM operated at the accelerating voltage of 200 kV. High-resolution TEM (HRTEM) images, high-angle annular dark-field scanning transmission electron microscopy (HAADF-STEM) images and chemical composition analysis were recorded using a Themis Z TEM with two aberration correctors and X-ray energy-dispersive spectroscopy (EDS). Scanning electron microscopy (SEM) images and the corresponding chemical composition analysis were obtained on a FEI NovaSEM 450 field emission SEM (FESEM) with a X-ray energy-dispersive spectroscopy. Power X-ray diffraction (XRD)

View Article Online DOI: 10.1039/C9NR02866B



patterns were recorded on a PANalytical X'Pert Pro MPD with Cu Kα radiation (λ = 1.5406 Å). The voltage and current employed were 40 KV and 40 mA, respectively. The X-ray photoelectron spectroscopy (XPS) was performed on an ESCALAB 250 instrument under ultrahigh vacuum ($10^{-9}$ Torr) using monochromated Al Kα radiation (hν = 1486.6 eV), all the binding energy were calibrated by the carbon peak (C 1s) at about 284.5 eV. The d-band center position was determined according to the formula in the range of 0 and -9 eV: $\int N(\varepsilon)\varepsilon d\varepsilon / \int N(\varepsilon) d\varepsilon$, where $N(\varepsilon)$ is the density of states (DOS), and all the spectra collected are corrected using the Shirley background. Nitrogen physisorption isotherms were recorded on an ASAP 2460 system at 77 K. 60 mg of AgPd-$Pt_{dilute}$ aerogels was transferred into the measuring cell and degassed in vacuum (323 K) for 24 h before analysis.

**Electrochemical measurements**

Electrochemical measurements were carried out in a standard three-electrode cell with CHI 660C electrochemical workstation (Shanghai Chenhua Apparatus, China). Glassy carbon electrode (GCE, diameter: 5 mm, area: 0.196 $cm^2$) was successively polished with 1.0, 0.3 and 0.05 μm alumina powder and ultrasonically cleaned in acetone and water prior to the surface coating. To prepare the working electrode, 1 mg of electrocatalysts were dispersed in 780 μL of ethanol, added with 20 μL of 5 wt% Nafion solution, and vigorously sonicated for half an hour to form a uniform catalyst suspension. Then, 5 μL of the catalysts suspension was dropped onto the glassy carbon electrode and dried naturally. The concentration and quality of different metals in the suspension were determined using a combination of inductively coupled plasma optical emission spectroscopy (ICP-OES) and EDS analyses. For comparison, the commercial Pt/C and Pd/C catalysts were used as the reference catalysts (Pt loading 20 wt. % and Pd loading 10 wt. %, respectively), the Pt or Pd loading was limited to 20.4 μg $cm^{-2}$. The electrochemical experiments for formate oxidation were performed with the catalyst deposited GCE as the working electrode, platinum gauze as the counter electrode and mercury-mercury oxide (MMO) Hg|HgO|(NaOH 1M) as the reference electrode. All potentials were scaled *versus* the reversible hydrogen electrode (RHE) by following the formula $E_{RHE} = E_{MMO} + 0.0198\ V + 0.05916 \times pH$. All electrochemical measurements were carried out at room temperature. The KOH solutions were deaerated using research-grade nitrogen for at least half an hour before use. For formate oxidation, the working electrode was subjected to different potential windows (from -0.1 V to 1.1, 1.2, and 1.3 V) at 50 mV $s^{-1}$ in 0.5 M KOH and 0.5 M HCOOK solution.

## Results and discussion

**Physical characterizations of pristine AgPd and AgPd-$Pt_{dilute}$ aerogels**

The trimetallic AgPd-$Pt_{dilute}$ aerogel was for the first time synthesized via a facile kinetically-controlled method in aqueous solution without any surfactants at 60°C (see Experimental Section for details), in which excess $NaBH_4$ was used as a strong reductant to realize a rapid and complete reduction process. As shown in Fig. 1a and Fig. S2 (Supporting Information), scanning electron microscopy (SEM) images show that the as-obtained AgPd-$Pt_{dilute}$ aerogel has the typical sponge nanostructure composed of interconnected ultrathin nanowires and abundance of hierarchical pores. By contrast, the as-synthesized bimetallic AgPd aerogel using the same method exhibits the quite different structure that features compactly fused irregular nanoparticles (Fig. S3, Supporting Information). Such morphology was also observed in other $Ag_xPd_y$ aerogels with different Ag/Pd molar ratios. However, once the same small amount of Pt precursor was introduced during the synthetic process, all the resultant $Ag_xPd_y$-$Pt_{dilute}$ aerogels possess the unique nanowire structure (Fig. S4, Supporting Information). Therefore, we propose that the dilute amount of Pt might act as an important structure directing agent in this work for the successful synthesis of ultrathin nanowires, which is a highly preferable nanostructure to effectively expose more active sites and stabilize the structure during the electrocatalytic process according to the recent researches.[25, 26] As can be seen from the transmission electron microscopy (TEM) image in Fig. 1b, the AgPd-$Pt_{dilute}$ nanowires are further observed to be necklace-like, which display well-defined particle profiles, suggesting their formation from the fusion of nanoparticles. It is deduced that the metal precursors can be instantly reduced by the excess $NaBH_4$ to create massive bare metal nuclei, which provides favorable nucleation sites for the growth of nanoparticles; the clean nanoparticles firstly collide and contact at the sites with high surface energy, and then self-assemble into 1D nanowires through atom diffusion. Selected area electron diffraction (SAED) pattern with clearly continuous diffraction rings evidences the highly-crystalline nature of AgPd-$Pt_{dilute}$ aerogel (Fig. 1b, inset). High-resolution TEM (HRTEM) images of two randomly-selected nanoparticles show the well-resolved lattice fringes, and the *d* spacing of 0.232 and 0.197 nm is between that of Ag(111), Pd(111), Pt(111) and Ag(200), Pd(200), Pt(200), respectively, suggesting the formation of trimetallic AgPdPt alloy (Fig. 1c). The corresponding fast Fourier transformation (FFT) patterns verify the single-crystalline structure of the fused nanoparticles.

Furthermore, we used the spherical-aberration-corrected TEM (Cs-corrected TEM) to fine-resolve the structure of AgPd-$Pt_{dilute}$ aerogel at the atomic level. As shown in Fig. 1d, large numbers of atomic steps and grain boundaries were clearly observed on the nanowires, which are dominated by low-coordinated atoms, serving as highly active spots for electrocatalytic reactions.[27-29] The elemental distribution was investigated by the high-angle annular dark-field (HAADF) STEM and energy-dispersive X-ray spectroscopy (EDS), the elemental maps show that Ag, Pd and Pt are all homogeneously distributed throughout the nanowires (Fig. 1e), as could further be proved by EDS line scan and the nearly constant Ag-L/(Pd-L+Pt-M) count ratio along the typical line (Fig. 1f). The atomic percentage of Ag, Pd and Pt in the pristine AgPd-$Pt_{dilute}$ aerogel based on the EDS analysis is determined to be 29.3, 62.4 and 8.3 at %, respectively, consistent with the result of inductively coupled plasma optical emission spectroscopy (ICP-OES) (Fig. S5 and Table S2, Supporting Information). Moreover, the EDS analysis on various bimetallic $Ag_xPd_y$ and trimetallic $Ag_xPd_y$-$Pt_{dilute}$ aerogels also matches well with the ICP-OES results and the stoichiometry of initial metal precursors, indicating that the suggested synthetic method in this work has the capacity for well controlling the

View Article Online
039/C9NR03266E

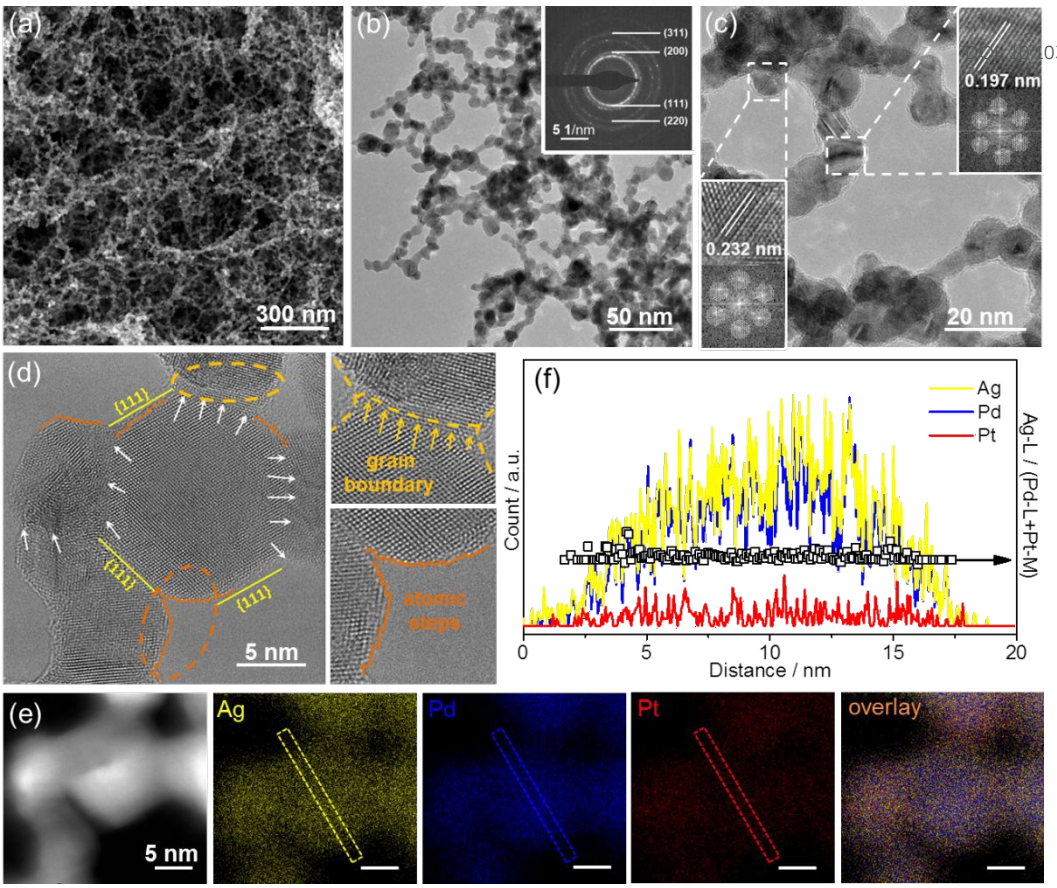


**Fig. 1** Physical characterizations of the as-synthesized AgPd-Pt$_{dilute}$ aerogel catalyst. (a) SEM image. (b) TEM image, inset is the SAED pattern. (c) HRTEM image of nanowires composed of fused highly-crystalline nanoparticles, insets show the magnified HRTEM images and corresponding FFT patterns recorded from the marked regions. (d) Cs-corrected HRTEM images of a representative nanowire. (e) HAADF-STEM image and high-resolution EDS elemental mappings of a single nanowire, all the scale bars in e) are 5 nm. (f) STEM-EDS line profiles and the corresponding Ag-L/(Pd-L+Pt-M) count ratio along the typical line marked in e).

composition of aerogels. Additionally, the XRD patterns of Ag$_x$Pd$_y$ and Ag$_x$Pd$_y$-Pt$_{dilute}$ aerogels exhibit well-defined diffraction peaks attributed to (111), (200), (220), and (311) planes for the face center cubic (fcc) structure (Fig. S6a,b, Supporting Information), and each of the peaks is located between the corresponding peaks of pure Pd/Pt and pure Ag. Compared to the standard diffraction patterns of Pd (JCPDS no.46-1043) and Pt (JCPDS no.04-0802), all of the diffraction peaks are shifted to lower angles, which is due to the permeation of larger Ag metal atoms into the Pd and/or Pt lattice to form the bimetallic AgPd and trimetallic AgPdPt alloys.[30]

The surface area and porosity properties of AgPd-Pt$_{dilute}$ aerogel was determined by the nitrogen adsorption/desorption analyses (Fig. S7, Supporting Information). The isotherms obtained at 77 K exhibit a type IV curve with some resemblance to a type II curve, suggesting the AgPd-Pt$_{dilute}$ aerogel with interlinked meso- and macroporous structures (Fig. S7a, Supporting Information). The surface area of AgPd-Pt$_{dilute}$ aerogel based on the Brunauer-Emmett-Teller (BET) model is 34.83 m$^2$ g$^{-1}$, which is comparable to those of previously reported aerogels prepared from the gelation of nanoparticle colloids.[31-33] As seen from Fig. S7b (Supporting Information), the pore-size distribution plot determined using the Barrett-Joyner-Halenda (BJH) model shows a wide range of pores from micropores, mesopores to marcopores in the AgPd-Pt$_{dilute}$ aerogel, and the cumulative volume plot indicates that the porosity is mainly from mesopores and macropores.[34] Such hybrid pores system is of high advantage for enhancing diffusion rates of molecules in catalytic reactions since the 10-50 nm pores can effectively minimizes the diffusion resistances in the catalyst layer.[35, 36]

**Physical characterizations of surface-restructured AgPd-Pt$_{dilute}$ aerogel**

Systematically physical characterizations were further carried out on the AgPd-Pt$_{dilute}$ aerogel that cycled to 1.3 V (referred to as AgPd-Pt$_{dilute}$-1.3) for 20 cycles in 0.5 M KOH + 0.5 M HCOOK electrolyte to examine the important surface variations induced by the electrochemical cycling with the large upper potential limit. Selecting 20 as the optimal potential cycle number here is based on our systematically electrochemical results (Fig. S8, Supporting Information). TEM images shown in Fig. 2a,b exhibit that the hierarchically porous nanostructure with high density of defects including atomic steps and grain boundaries are well preserved during the high-potential-driven electrochemical testing, indicating that the potential cycling process does not destroy the nanostructure of AgPd-Pt$_{dilute}$ aerogel. The primary and the most significant change observed by Cs-corrected TEM is the locally

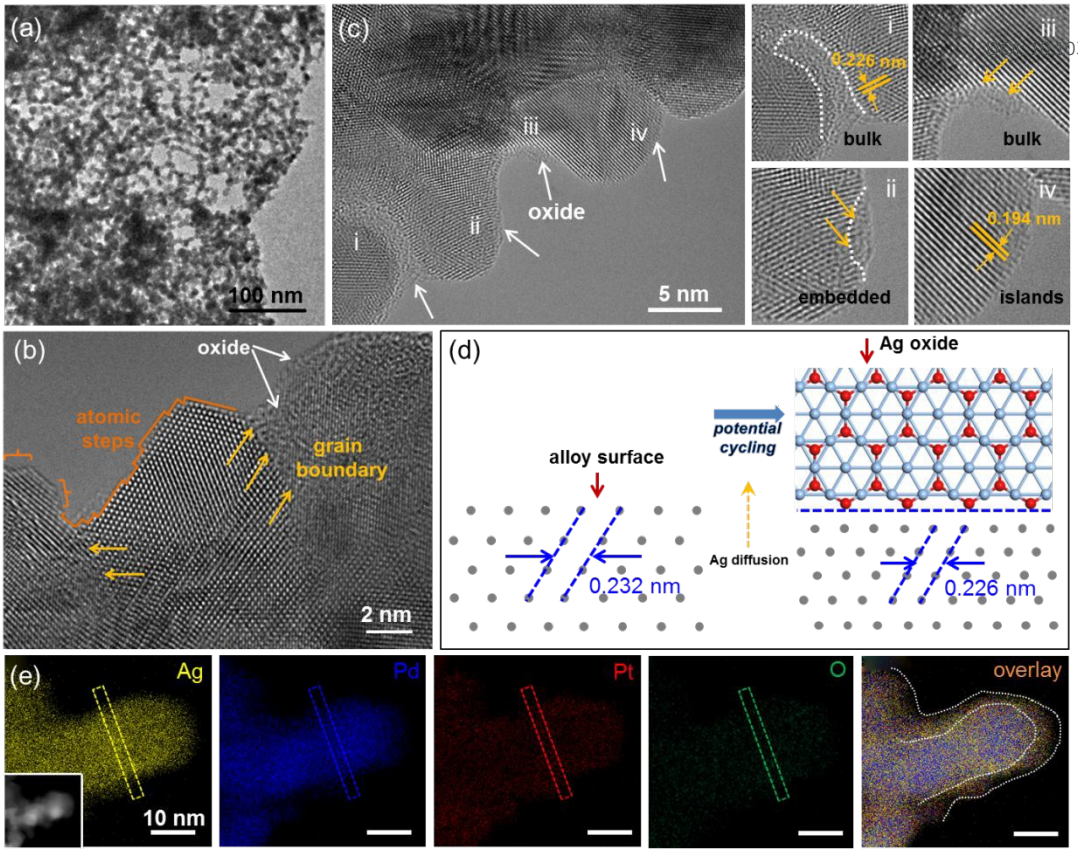


**Fig. 2** Physical characterizations of the surface-restructured AgPd-Pt$_{dilute}$-1.3 aerogel electrocatalyst. (a) TEM image. (b) Cs-corrected HRTEM image of a randomly-selected area on the nanowire surface. (c) Cs-corrected HRTEM image of some representative branches. (i-iv) Magnified HRTEM images of amorphous metal oxides with different morphologies obtained from regions i, ii, iii, and iv marked in c). (d) Atomic illustration of AgPd-Pt$_{dilute}$-1.3 aerogel before and after potential cycling. (e) HAADF-STEM image and high-resolution EDS elemental mappings of a single nanowire, all the scale bars are 10 nm.

formed amorphous oxide species with different morphologies on and within the AgPd-Pt$_{dilute}$-1.3 nanowires (bulk, embedded, and islands, Fig. 2c) that are not detected in the pristine AgPd-Pt$_{dilute}$ aerogel (Fig. 1d), which are identified as mostly $Ag_2O$ via the following XPS techniques. The XRD pattern of the AgPd-Pt$_{dilute}$-1.3 aerogel did not show any new diffraction peaks relative to the pristine AgPd-Pt$_{dilute}$ aerogel (Fig. S6c, Supporting Information), further indicating the amorphous nature of the oxides. More importantly, it can be calculated that the *d* spacings of interior layers adjacent to the surface oxides are 0.226 and 0.194 nm (i, iv in Fig. 2c), which are closer to the values of Pd(111), Pt(111) and Pd(200), Pt(200), respectively, interestingly implying that the interface lacks Ag atoms in comparison with the trimetallic PdAgPt alloys (Fig. 1c). Fig. 2d further provide a vivid visualization that the formed oxides mainly come from the Ag diffusion outward the surface and then being oxidized during the high-potential cycling process, resulting in the most active PdPt-enriched surface accompanied with locally distributed $Ag_2O$ domains. A closer look into i-iv insets in Fig. 2c finds that the *in situ* generated amorphous oxides on the AgPd-Pt$_{dilute}$-1.3 surface exhibit an atomically intimate contact with the substrate (red arrows), which ensures the favorable interactions between oxides with active metals for the electrocatalytic process. Moreover, the EDS elemental maps shown in Fig. 2e display a clear Ag-segregation composition distribution on surface, which confirms the outward diffusion of Ag element and that oxides on AgPd-Pt$_{dilute}$-1.3 surface possess more $Ag_xO$. All these aforementioned results demonstrate a novel and unexplored surface restructuring process of the pristine AgPd-Pt$_{dilute}$ trimetallic alloys into atomically coupled amorphous oxide/active PdPt composite during the electrochemical testing with the large upper potential limit of 1.3 V, which might significantly promote the electrocatalytic reactions due to the favorable interactions between amorphous oxide and active metal species.

X-ray photoelectron spectroscopy (XPS) was performed to investigate the variations of element chemical state and electronic structure of the AgPd-Pt$_{dilute}$ aerogels that cycled to different upper potential limit (1.1, 1.2 and 1.3 V, referred to as AgPd-Pt$_{dilute}$-1.1, AgPd-Pt$_{dilute}$-1.2, AgPd-Pt$_{dilute}$-1.3, respectively). As shown in Fig. 3a, the high-resolution Ag 3d spectra of different aerogels show two peaks assigned to Ag $3d_{5/2}$ and Ag $3d_{3/2}$, and be further split into two doublets, which are associated with $Ag^0$ and $Ag^+$ chemical states. It can be seen that almost no Ag oxides exist on the AgPd-Pt$_{dilute}$-1.1 surface, while the Ag oxides are gradually present with enlarging the upper potential limit. The peak at 368.4 eV for AgPd-Pt$_{dilute}$-1.2 and peak at 367.7 eV for AgPd-Pt$_{dilute}$-1.3 suggest that the

View Article Online
DOI: 10.1039/C9NR03266E

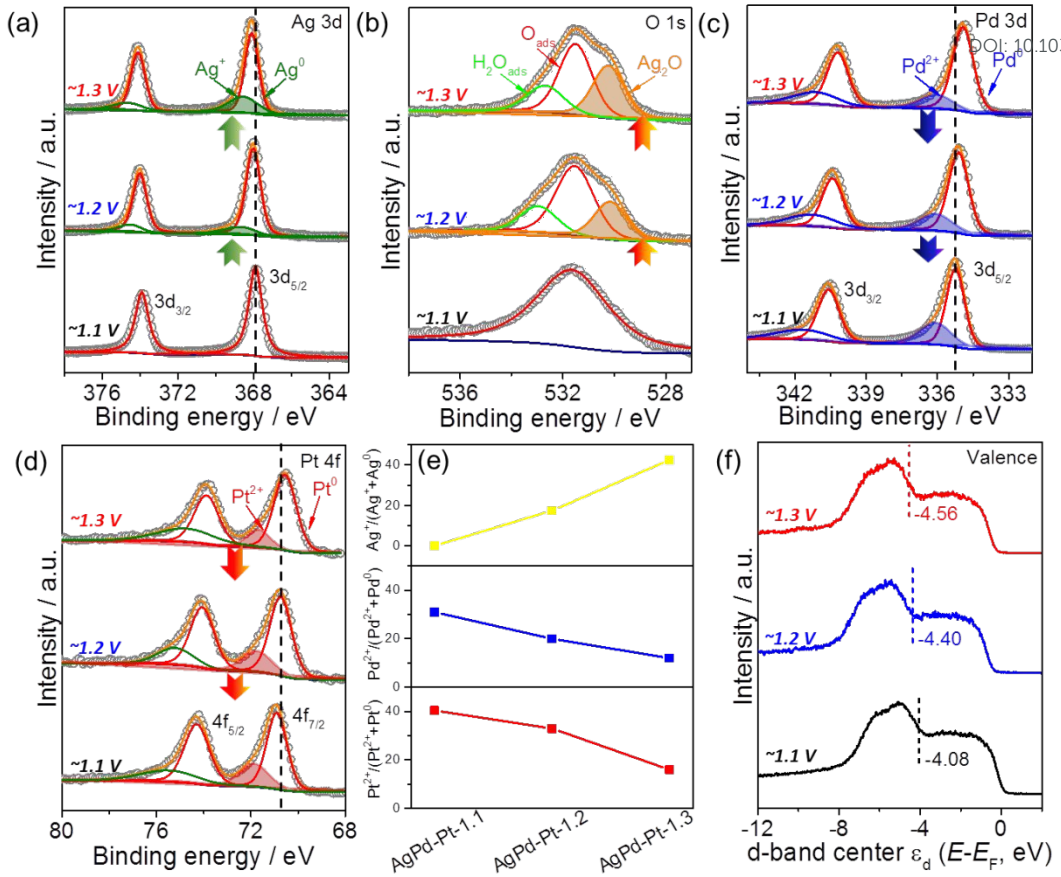


**Fig. 3** XPS analysis of the AgPd-Pt$_{dilute}$-1.1, AgPd-Pt$_{dilute}$-1.2 and AgPd-Pt$_{dilute}$-1.3 catalysts. (a-d) High-resolution spectra of (a) Ag 3d, (b) O 1s, (c) Pd 3d, and (d) Pt 4f, the dashed lines in a,c,d) refer to the peak positions of the binding energy for the pristine AgPd-Pt$_{dilute}$ aerogel. (e) Surface compositional comparison of $Ag_2O$, PdO and PtO in different catalysts. (f) Surface valence band spectra, the dashed lines indicate the specific position of the d-band center relative to the Fermi level.

oxidized silver species are mainly $Ag_2O$.[37] To confirm the presence of $Ag_2O$ species in a more convincing way, O 1s spectra were further measured (Fig. 3b). The O 1s spectra of both AgPd-Pt$_{dilute}$-1.2 and AgPd-Pt$_{dilute}$-1.3 exhibit the new peaks at 529.4 eV compared to that of the AgPd-Pt$_{dilute}$-1.1, which is assigned to the $Ag_2O$ according to the previous report.[38, 39] As can be seen in Fig. 3e, the content of $Ag_2O$ species in the cycled AgPd-Pt$_{dilute}$ aerogels significantly increases with enlarging the upper potential limit. When the upper potential limit is enlarged from 1.1 V to 1.2 V and 1.3 V, the atomic ratio of $Ag_2O$ ($Ag^+/(Ag^+ + Ag^0)$) sharply increases from 0% to 17.4% and 42.5%, respectively. The Pd $3d_{5/2}$ (Pt $4f_{7/2}$) can be also split into one doublet, which is associated with $Pd^0$ ($Pt^0$) and $Pd^{2+}$ ($Pt^{2+}$) chemical states (Fig. 3c,d). As a sharp contrast, it is notable that the ratios of PdO ($Pd^{2+}/(Pd^{2+}+Pd^0)$) and PtO ($Pt^{2+}/(Pt^{2+}+Pt^0)$) intriguingly decrease with the upper potential limit enlarging from 1.1 to 1.3 V, implying that Pd and Pt oxides are gradually converted into their metallic state on surface during the potential cycling (Fig. 3c-e). These interesting XPS findings further confirm the metallic PdPt-enriched surface with *in situ* formed $Ag_2O$ species on restructured AgPd-Pt$_{dilute}$ surface, which agrees well with the HRTEM results shown in Fig. 2c,d. The remarkably increased $Ag_2O$ species and decreased Pd an Pt oxides on surface under the high-potential cycling process can be explained by the surface energy of oxides and the cyclic voltammetry (CV) in the following electrochemical characterizations.[40] According to the Pourbaix diagram, the fact that Ag oxides in alkaline media are more stable than the Pd and Pt oxides gives rise to the driving force for oxidizing more Ag on the AgPd-Pt$_{dilute}$ surface.[41, 42] Moreover, it can be also noted that the Ag 3d peaks in the surface-restructured AgPd-Pt$_{dilute}$-1.2 and AgPd-Pt$_{dilute}$-1.3 aerogels are gradually shifted to higher binding energies in comparison with that in the AgPd-Pt$_{dilute}$-1.1, while binding energies of Pd 3d and Pt 4f are gradually shifted to lower values, which fully indicates the efficient charge transfer from Ag to Pd and Pt, leading to an electron-rich region on the Pd/Pt and then the downshift of d-band center in the restructured AgPd-Pt$_{dilute}$ aerogels. Impressively, the most positive shift of Ag 3d and the most negative shifts of Pd 3d and Pt 4f were observed on the AgPd-Pt$_{dilute}$-1.3 aerogel, suggesting the higher tendency of charge transfer, which provides strong supports for the presence of vigorous interaction between *in situ* formed oxides and metals.[36, 43] Valence band spectra (VBS) were further performed to study the modification of electronic structures in the surface-restructured AgPd-Pt$_{dilute}$ electrocatalysts. As revealed in Fig. 3f, the d-band center in the AgPd-Pt$_{dilute}$-1.3 is calculated to be -4.56 eV, much farther away from the Fermi level compared with that in AgPd-Pt$_{dilute}$-1.1 (-4.08 eV) and AgPd-Pt$_{dilute}$-1.2 (-4.40 eV), which evidences the effective modulation of electronic structure in AgPd-Pt$_{dilute}$ aerogels after the

View Article Online
DOI: 10.1039/C9NR03266E

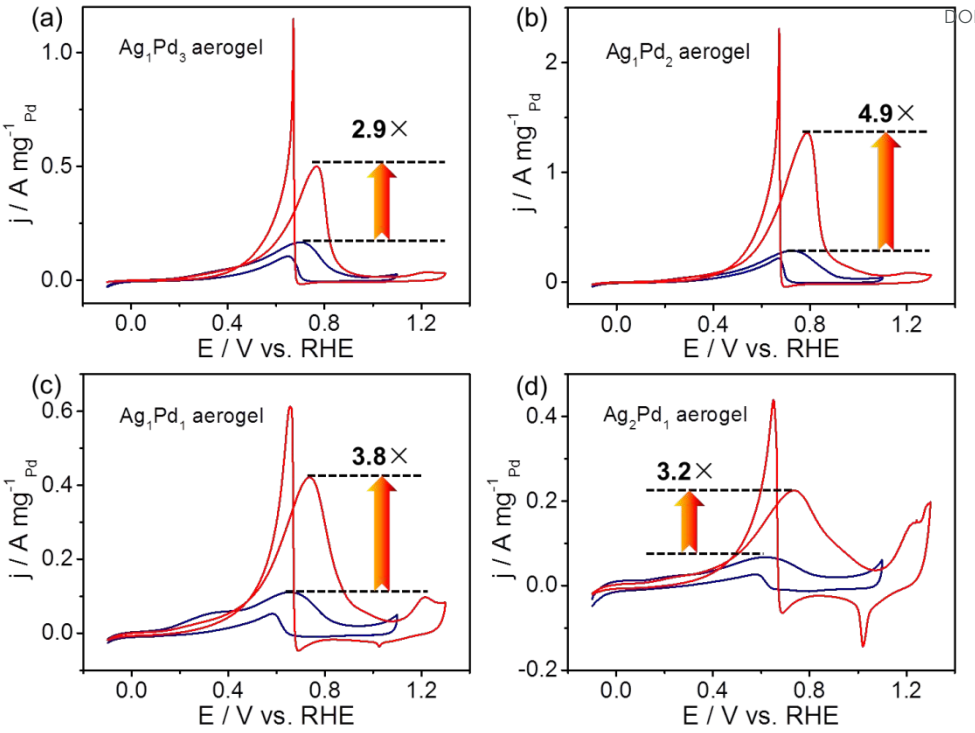


**Fig. 4** CV curves of various AgPd aerogel electrocatalysts with different Ag/Pd molar ratio for FOR in 0.5 M KOH + 0.5 M HCOOK solution at a conventional small (-0.1~1.1 V, blue line) and large (-0.1~1.3 V, red line) potential window.

high-potential-driven surface restructuring strategy. The more favorable downshift of the d-band center in the AgPd-Pt$_{dilute}$-1.3 indicates the efficiently weakened chemisorption strength of $H_{ad}$ intermediates on PdPt surfaces, leading to the much enhanced activity of every active sites for FOR.[4, 12]

**Electrocatalytic properties of pristine and surface-restructured aerogels**

The electrocatalytic formate oxidation reaction (FOR) activity of bimetallic $Ag_xPd_y$ aerogels with different compositions was first investigated by CV in $N_2$-saturated 0.5 M KOH + 0.5 M HCOOK solution. Fig. 4 shows the representative CV curves of different AgPd aerogel catalysts for FOR with a conventional (-0.1~1.1 V) and a large (-0.1~1.3 V) potential window. It can be seen from CV curves recorded with the upper potential limit of 1.1 V that all AgPd aerogels exhibit the obvious electrocatalytic activity for FOR. Based on the mass loading of Pd, the mass peak current density of FOR is calculated to be 0.17, 0.28, 0.11 and 0.07 A $mg_{Pd}^{-1}$ for $Ag_1Pd_3$, $Ag_1Pd_2$, $Ag_1Pd_1$ and $Ag_2Pd_1$ aerogels, respectively, and the $Ag_1Pd_2$ aerogel catalyst shows the best FOR activity among different $Ag_xPd_y$ aerogels. Most intriguingly, when the upper potential limit is enlarged to 1.3 V during the electrochemical testing, the corresponding CV curves show that the oxidation currents of all these four catalysts for FOR are significantly improved, and the final mass peak current is 2.9, 4.9, 3.8 and 3.2 times higher than the values measured with the potential window of -0.1~1.1 V for $Ag_1Pd_3$, $Ag_1Pd_2$, $Ag_1Pd_1$ and $Ag_2Pd_1$, respectively (Table S3, Supporting Information). It can be noted that the $Ag_1Pd_2$ aerogel exhibits the largest activity improvement and achieves the highest oxidation current towards FOR among various AgPd aerogels. Therefore, it is concluded that only the appropriate Ag content in the AgPd aerogel catalyst benefits to maximize the activity improvement.

Based on the optimized bimetallic AgPd aerogel catalyst, we further investigated the electrocatalytic FOR performance of trimetallic AgPd-Pt$_{dilute}$ aerogel, and the result was also compared with those of bimetallic AgPd, AgPt and commercial Pd/C catalysts. The representative CV curves of different catalysts for FOR recorded with the upper potential limit of 1.1 V are shown in Fig. 5a. It can be seen that the mass peak current density increases in the sequence: AgPt (0.16 A $mg_{Pt}^{-1}$) < AgPd (0.28 A $mg_{Pd}^{-1}$) < Pd/C (0.59 A $mg_{Pd}^{-1}$) < AgPd-Pt$_{dilute}$ (0.67 A $mg_{Pd+Pt}^{-1}$). The AgPd-Pt$_{dilute}$ aerogel catalyst shows the best current density for FOR, which is 2.4 and 1.2 times higher than that of bimetallic AgPd and the commercial Pd/C catalysts, respectively. Since Pt has very limited activity for FOR,[4, 11] as manifested in the much lower current densities on the AgPt and Pt/C in this work (Fig. S9 and S10, Supporting Information), the FOR activity of AgPd-Pt$_{dilute}$ should mainly result from the Pd active sites. The much higher FOR current density on the trimetallic AgPd-Pt$_{dilute}$ aerogels relative to the bimetallic AgPd is ascribed to the favorable nanoporous structure of AgPd-Pt$_{dilute}$ in the presence of Pt with more exposed active sites. On the other hand, although the Pt/C catalyst exhibits the low catalytic current density, its onset and peak potentials for FOR was observed strikingly much more negative than those of Pd/C, suggesting that the incorporation of Pt would effectively improve the electrocatalytic kinetics of Pd-based catalysts.[11] As expected, the trimetallic AgPd-Pt$_{dilute}$ with a small amount of Pt has the most negative onset potential for FOR among all of tested catalysts, about 200 mV lower than that of bimetallic

View Article Online
DOI: 10.1039/C9NR03266E

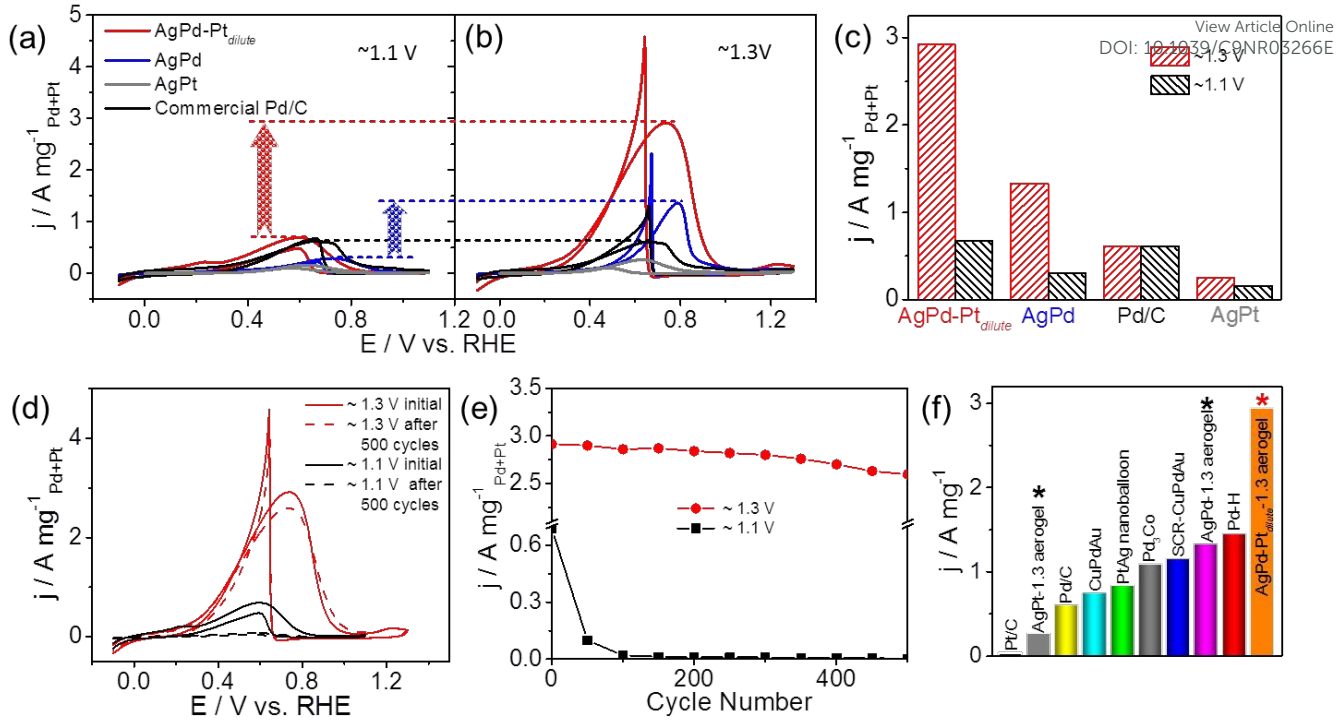


**Fig. 5** CV curves of AgPd-Pt$_{dilute}$, AgPd, AgPt and commercial Pd/C electrocatalysts for FOR in 0.5 M KOH + 0.5 M HCOOK solution with a (a) conventional small (-0.1~1.1 V) and (b) large (-0.1~1.3 V) potential window at 50 mV s$^{-1}$, and (c) comparison of mass peak current density. (d) CV curves before and after successive scans of 500 cycles with different potential windows. (e) Durability comparison of AgPd-Pt$_{dilute}$-1.1 and AgPd-Pt$_{dilute}$-1.3 as a function of cycle numbers. (f) Peak current density of surface-restructured AgPd-Pt$_{dilute}$-1.3, AgPd-1.3 and AgPt-1.3 aerogels compared with some recently reported FOR electrocatalysts.

AgPd aerogel catalyst.

Most importantly, the FOR activity of trimetallic AgPd-Pt$_{dilute}$ aerogel catalyst undergoes an unusual large enhancement when the upper potential limit is enlarged to 1.3 V during the electrochemical testing. As shown in Fig. 5b,c, the mass peak current density of AgPd-Pt$_{dilute}$-1.3 aerogel remarkably increases from 0.67 to 2.94 A mg$_{Pd+Pt}^{-1}$ with the upper potential limit increasing from 1.1 to 1.3 V, inducing a 4.4-fold further activity enhancement for FOR. Simultaneously, the onset potential of the AgPd-Pt$_{dilute}$-1.3 aerogel exhibits a further significant 60 mV negative shift compared with that of AgPd-Pt$_{dilute}$-1.1. Such high-potential-driven activity enhancement is so outstanding that the AgPd-Pt$_{dilute}$-1.3 aerogel exhibits about 5 times higher mass activity than the commercial Pd/C, demonstrating a record-high FOR mass activity and low onset/peak potentials reported to date (Table S3, S4 Supporting Information). Moreover, compared with the markedly enhanced activity on the AgPd-1.3, the AgPt-1.3 catalyst only shows a slight FOR activity enhancement, further certifying that Pd is the primary active sites for FOR. Besides, the electrochemical FOR activity on other Ag$_x$Pd$_y$-Pt aerogels was further systematically investigated by CV with the upper potential limit of 1.1 and 1.3 V (Fig. S11 and Table S3, Supporting Information). As shown, the mass peak current of Ag$_1$Pd$_3$-Pt, Ag$_1$Pd$_2$-Pt (AgPd-Pt$_{dilute}$), Ag$_1$Pd$_1$-Pt and Ag$_2$Pd$_1$-Pt catalysts shows a 2.7-, 4.4-, 3.2- and 3.0-fold improvement for FOR, respectively, with the upper potential limit enlarged from 1.1 to 1.3 V. In particular, the Ag$_1$Pd$_2$-Pt catalyst with the Pd/Ag atomic ratio of 1/2 exhibits the largest current enhancement and the highest FOR activity among all the tested Ag$_x$Pd$_y$-Pt aerogels, which is consistent with the results observed on bimetallic Ag$_x$Pd$_y$ catalysts (Fig. 4), suggesting the Ag/Pd atomic ratio in both Ag$_x$Pd$_y$ and Ag$_x$Pd$_y$-Pt$_{dilut}$ plays a crucial role to achieve the largest activity improvement for FOR by the high-potential-driven surface restructuring process. We have also conducted the cycling stability on the trimetallic AgPd-Pt$_{dilute}$ aerogels by the successive 500 potential cycles with the different upper potential limits. The AgPd-Pt$_{dilute}$-1.3 exhibits the negligible mass activity degradation after 500 successive cycling, while the AgPd-Pt$_{dilute}$-1.1 undergoes a drastic decrease of peak current density over the first 100 cycles (Fig. 5d,e). After 500 cycles, the peak current density of AgPd-Pt$_{dilute}$-1.3 and AgPd-Pt$_{dilute}$-1.1 finally decays by 10 and 96 % for FOR, respectively, suggesting that the high-potential-driven surface restructuring also benefits the electrocatalytic FOR stability of AgPd-Pt$_{dilute}$ aerogels. More intriguingly, it is noted that the oxidation current of AgPd-Pt$_{dilute}$-1.3 shows a slight increase at the initial potential cycles (red line, Fig. 5e), which can be attributed to the abundant active sites and the optimized binding energy of adsorbed hydrogen intermediates on AgPd-Pt$_{dilute}$-1.3, which effectively accelerates the oxidation and desorption rate of hydrogen, releasing more fresh active sites for the accessibility of subsequent formate molecules. This phenomenon has also been reported in recent literature.[44] To obtain a straightforward comparison, the mass peak current density of AgPd-Pt$_{dilute}$-1.3 aerogel was compared with those of recently reported FOR electrocatalysts in Fig. 5f. Our results confirm that the surface-restructured AgPd-Pt$_{dilute}$-1.3 aerogel represents the best electrocatalyst towards FOR.

View Article Online
DOI: 10.1039/C9NR03266E



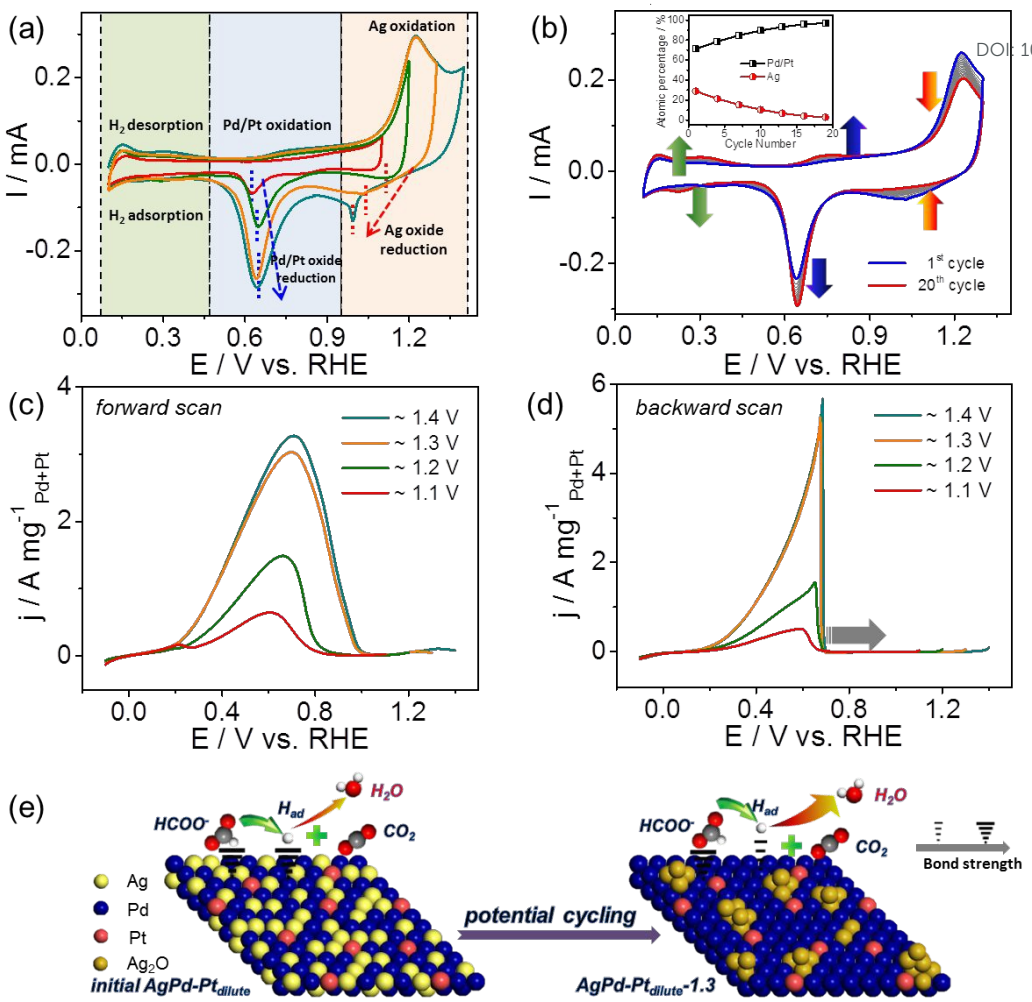


**Fig. 6** (a) Representative CV curves of AgPd-Pt$_{dilute}$ aerogel recorded in 0.5 M KOH solution with the different upper potential limit (1.1, 1.2, 1.3 and 1.4 V). (b) CV evolution of AgPd-Pt$_{dilute}$ aerogel catalyst from 1$^{st}$ to 20$^{th}$ potential cycles, inset shows the composition variation on surface as a function of cycle number during the continuous potential cycling process. (c) Forward scan curves of CV for FOR on AgPd-Pt$_{dilute}$ aerogel recorded immediately after cycling in 0.5 M KOH solution for 20 cycles with different upper potential limit. (d) Corresponding backward scan curves of CV for FOR on AgPd-Pt$_{dilute}$ aerogel with different upper potential limit. (e) Schematic illustration of pristine AgPd-Pt$_{dilute}$ trimetallic alloy to surface-restructured AgPd-Pt$_{dilute}$-1.3 transformation. Large red arrow on the AgPd-Pt$_{dilute}$-1.3 indicates the higher production of $H_2O$ from adsorbed hydrogen.

**Origins of great activity improvement on high-potential-driven restructured aerogels**

To explore the real promoting factor in the surface-restructured AgPd-Pt$_{dilute}$-1.3 for the greatly improved FOR performance, the AgPd-Pt$_{dilute}$ aerogels were firstly cycled for continuous potential cycles in 0.5 M KOH solution at different potential windows (-0.1~1.1, ~1.2, ~1.3 and 1.4 V) for a stable restructured electrode state, and then directly evaluated their FOR activities in 0.5 M KOH + 0.5 M HCOOK solution. The CV curves of AgPd-Pt$_{dilute}$ aerogels cycled with different upper potential limit in 0.5 M KOH solution is illustrated in Fig. 6a. When the AgPd-Pt$_{dilute}$ is scanned to 1.1 V, only one redox peaks at 0.75/0.63 V were observed, corresponding to the redox process of Pd and Pt.[45-47] As the upper potential limit increases up to 1.2, 1.3 and 1.4 V, another pair of redox peaks begins to appear. The peak at 1.23 V has been reported to be responsible for the formation of $Ag_2O$, and the cathodic peak at 1.0~1.1 V is attributed to the reduction of $Ag_2O$ to metallic Ag.[37, 48] Through comparing the integral areas of reduction peaks of $Ag_2O$, it can be seen that the larger upper potential limit applied during the electrochemical process would induce the greater redox process of Ag on the AgPd-Pt$_{dilute}$ aerogel surface. We also found that the reduction peaks of Ag oxide are relatively weak in comparison with the easily visible oxidation peaks in the CVs. Such irreversible reduction of Ag oxide indicates that more $Ag_2O$ species could be *in situ* stably formed on surface during the electrochemical testing in alkaline environment.[42, 49, 50] Moreover, it is noteworthy that the reduction peaks of Pd/Pt oxides (blue dashed line) are gradually shifted to positive direction with increasing the upper potential limit, while those of Ag oxide (red dashed line) are reversely shifted to negative direction, which indicates that the higher upper potential limit induces much easier reduction of Pd/Pt oxides and more difficult reduction of Ag oxides, confirming the effective

View Article Online
DOI: 10.1039/C9NR02665F



surface reconstruction by the high-potential cycling. Significantly, the continuous CV curves from 1st to 20th potential cycles on AgPd-Pt$_{dilute}$ aerogel recorded in 0.5 M KOH electrolyte were further investigated. As shown in Fig. 6b, the CV curves of the initial first and the following cycling show that the Pd/Pt oxides reduction peaks (blue arrows) gradually increase with increasing the potential cycles, implying the gradual formation of Pd/Pt enriched surface after the cycling process, as could be further confirmed by the increase of hydrogen adsorption/desorption peaks (green arrows). By contrast, the Ag oxides reduction peaks accordingly decrease, suggesting the reduced metallic Ag on catalyst surface. The composition evolution on AgPd-Pt$_{dilute}$ catalyst during the potential cycling is displayed in inset in Fig. 6b, which provides more convincing evidence for understanding the formation of metallic PdPt-enriched surface with remarkably increased $Ag_2O$ on AgPd-Pt$_{dilute}$-1.3 catalyst from an electrochemical standpoint, which is well consistent with the TEM and XPS results.

The forward potential scans for FOR on the AgPd-Pt$_{dilute}$ electrocatalyst recorded immediately after cycling in 0.5 M KOH at different potential windows were firstly studied. As shown in Fig. 6c, the larger upper potential limit the electrocatalyst is cycled to, the better catalytic activity for FOR is achieved. However, when the upper potential limit is continuously enlarged to 1.4 and much larger values (not shown here) during the CV testing, the corresponding FOR activity only shows the very slight improvement. Therefore, the optimized potential window for achieving the largest activity improvement on AgPd-Pt$_{dilute}$ in this work is determined to be -0.1~1.3 V. Impressively, the mass activity of AgPd-Pt$_{dilute}$-1.3 aerogel for FOR is 4.6 and 2.0 times higher than that of AgPd-Pt$_{dilute}$-1.1 and AgPd-Pt$_{dilute}$-1.2, which is in accordance with the results shown in Fig. 5a,b. Since the redox process of Pd and Pt makes no contributions to the activity improvement, as manifested in the no visible oxidation activity change on the monometallic Pd/C and Pt/C catalysts with the upper potential limit enlarging from 1.1 V to 1.3 V (Fig. S12, Supporting Information). It can be concluded that the redox process of Ag with increased *in situ* formed $Ag_2O$ species during the high-potential-driven restructuring process facilitates the achievement of greatly promoted FOR performance. On the other hand, the corresponding backward potential scans for FOR are shown in Fig. 6d. Intriguingly, one can find that the backward scan peak currents are significantly enhanced as the upper potential limit is enlarged. Given that there is no well-known poisoning intermediates (such as CO) generated on Pd during FOR process in alkaline media, such enhanced peak current indicates much higher activity for FOR. Moreover, the onset potentials of backward scan peaks were further observed to be positively shifted with increasing the upper potential limit, which is highly consistent with the positive shift of reduction peaks of Pd/Pt oxides shown in Fig. 6a. These results strongly demonstrate that the cycling process with higher upper potential limit endows the AgPd-Pt$_{dilute}$ aerogel with a large degree of PdPt enriched surface, which exposes much more active sites and results in the remarkably improved FOR activity. Besides, we have also investigated the FOR activity variations of as-synthesized PdCu aerogel catalyst recorded with different potential windows, as shown in Fig. S13 (Supporting Information), the oxidation current does not undergo any improvement with the upper potential limit enlarging from 1.1 V to 1.3 V, certifying the unique promoting role of Ag redox process over other metals for FOR. Meanwhile, the negligible activity enhancement observed on PdCu electrocatalyst recorded under the same experimental conditions further excludes the possibility that the surface roughness during the high-potential cycling leads to the significantly enhanced FOR activity on AgPd-Pt$_{dilute}$ electrocatalyst. To the best of author's knowledge, this research represents the first example of reporting the *in-situ* high-potential-driven restructuring strategy during the electrochemical testing to engineering AgPd-Pt$_{dilute}$ electrocatalyst with greatly enhanced FOR performance in alkaline media.

Through the above investigations, we have developed a novel *in-situ* high-potential-driven restructuring strategy during the electrochemical testing to engineering AgPd-Pt$_{dilute}$ catalyst for FOR in alkaline media. The unprecedented electrocatalytic FOR performance of the surface-restructured AgPd-Pt$_{dilute}$ aerogel could be attributed to the following reasons. Firstly, the AgPd-Pt$_{dilute}$ aerogel surface undergoes a remarkably structural and compositional restructuring process by extending the upper potential limit to the Ag redox region during the electrochemical testing, which strikingly transforms AgPd-Pt$_{dilute}$ catalyst from pristine trimetallic alloy into metallic Pd/Pt enriched surface atomically coupled with amorphous $Ag_2O$, providing more exposed active sites for formate oxidation process (Fig. 6e). Secondly, the strong interactions between amorphous $Ag_2O$ species and PdPt-enriched active sites lead to the effectively modified electronic band structure of AgPd-Pt$_{dilute}$ aerogel. The favorable downshift of the d-band center weakens the binding energy of adsorbed hydrogen on Pd,[2, 51] markedly improving the activity of every active sites towards FOR (Fig. 3f and Fig. 6e). Such a more facile *in-situ* strategy fully satisfies the criteria of designing a high-performance electrocatalyst by simultaneously increasing the number of active sites and improving specific activity of every sites. Moreover, previous investigations have demonstrated that the amorphous phases usually exhibit more prominent effect on catalytic properties than their crystalline counterparts,[23, 24] thus the presence of amorphous $Ag_2O$ in this work is further beneficial for the improvement of FOR performance. Thirdly, the inherent properties of AgPd-Pt$_{dilute}$ aerogel, such as 3D hierarchically nanoporous structure, high surface area and ample low-coordinated active sites, along with the good electronic conductivity of *in situ* formed $Ag_2O$ species, also contributes to facilitate the mass and electron transfer rate for enhancing the electrocatalytic FOR.

## Conclusions

In summary, for the first time, we report an *in-situ* high-potential-driven restructuring strategy to intriguingly induce structural and compositional reconstruction on a new class of ternary AgPd-Pt$_{dilute}$ aerogel for FOR in alkaline media, in which the large upper potential limit during the electrochemical CV testing is judiciously enlarged to the Ag redox region. The unique Ag element outward diffusion under the high-potential cycling induces the ternary AgPd-Pt$_{dilute}$ aerogel electrocatalyst transformation from alloys into metallic PdPt-enriched surface atomically coupled locally-distributed amorphous $Ag_2O$ species, which results in the much more exposed

active sites, highly advantageous interfacial interactions and then the optimized electronic structure for FOR. As a result, the surface-restructured AgPd-Pt$_{dilute}$-1.3 aerogel electrocatalyst achieves a record-high catalytic activity and stability among all recently reported FOR electrocatalysts to date. Specifically, the AgPd-Pt$_{dilute}$-1.3 aerogel yields a mass peak current density of 2.94 A $mg_{Pd+Pt}^{-1}$, which is 5 times higher than that of the commercial Pd/C catalyst. It also exhibits the remarkably improved FOR stability with the negligible activity degradation after 500 potential cycles. This is the first report for emphasizing the unique and critical role of Ag redox process in electrocatalysts for the giant catalytic activity improvement. It is believed that the key finding of our work should provide more insights into the design of advanced electrocatalysts for various reactions in future energy storage/conversion devices.

## Conflicts of interest

There are no conflicts to declare.

## Acknowledgements

This work was supported by the National Natural Science Foundation of China (grant nos. 51874243, 51271148 and 50971100), the Research Fund of State Key Laboratory of Solidification Processing in China (grant no. 150-ZH-2016), the Aeronautic Science Foundation Program of China (grant no. 2012ZF53073), the Project of Transformation of Scientific and Technological Achievements of NWPU (grant no. 19-2017), the Doctoral Fund of Ministry of Education of China (grant no. 20136102110013), and the Open Fund of State Key Laboratory of Advanced Technology for Materials Synthesis and Processing (Wuhan University of Technology, grant no. 2018-KF-18). We would like to thank the Analytical & Testing Center of Northwestern Polytechnical University for SEM and TEM characterizations.

## Notes and references

1 C. Bianchini and P. K. Shen, *Chem. Rev.*, 2009, **109**, 4183-4206.
2 L. Chen, L. Lu, H. Zhu, Y. Chen, Y. Huang, Y. Li and L. Wang, *Nat. Commun.*, 2017, **8**, 14136.
3 Z. Chen, J. Zhang, Y. Zhang, Y. Liu, X. Han, C. Zhong, W. Hu and Y. Deng, *Nano Energy*, 2017, **42**, 353-362.
4 X. Yu and A. Manthiram, *Appl. Catal. B-Environ.*, 2015, **165**, 63-67.
5 L. An and R. Chen, *J. Power Sources*, 2016, **320**, 127-139.
6 J. L. Haan, O. Muneeb and J. Estrada, in *Anion Exchange Membrane Fuel Cells: Principles, Materials and Systems*, eds. L. An and T. S. Zhao, Springer International Publishing, Cham, 2018, pp. 33-77.
7 J. Jiang and A. Wieckowski, *Electrochem. Commun.*, 2012, **18**, 41-43.
8 H.-H. Li, Q.-Q. Fu, L. Xu, S.-Y. Ma, Y.-R. Zheng, X.-J. Liu and S.-H. Yu, *Energy Environ. Sci.*, 2017.
9 D. Strmcnik, M. Uchimura, C. Wang, R. Subbaraman, N. Danilovic, D. van der Vliet, A. P. Paulikas, V. R. Stamenkovic and N. M. Markovic, *Nat. Chem.*, 2013, **5**, 300.
10 X. Lu, Y. Wu, X. Yuan and H. Wang, *Angew. Chem. Int. Ed.*, DOI:10.1002/anie.201814257.
11 S.-H. Han, H.-M. Liu, J. Bai, X. L. Tian, B. Y. Xia, J.-H. Zeng, J.-X. Jiang and Y. Chen, *ACS Appl. Energy Mater.*, 2018, **1**, 1252-1258.
12 M. Choun, K. Ham, D. Shin, J. K. Lee and J. Lee, *Catal. Today*, 2017, **295**, 26-31.
13 R. Ferrando, J. Jellinek and R. L. Johnston, *Chem. Rev.*, 2008, **108**, 845-910.
14 J. Noborikawa, J. Lau, J. Ta, S. Hu, L. Scudiero, S. Derakhshan, S. Ha and J. L. Haan, *Electrochim. Acta*, 2014, **137**, 654-660.
15 S. Sankar, G. M. Anilkumar, T. Tamaki and T. Yamaguchi, *ACS Appl. Energy Mater.*, 2018, **1**, 4140-4149.
16 Y. Li, Y. He and W. Yang, *J. Power Sources*, 2015, **278**, 569-573.
17 H. Wang and H. D. Abruña, *J. Am. Chem. Soc.*, 2017, **139**, 6807-6810.
18 S. Lu and Z. Zhuang, *J. Am. Chem. Soc.*, 2017, **139**, 5156-5163.
19 F. Tao, M. E. Grass, Y. Zhang, D. R. Butcher, J. R. Renzas, Z. Liu, J. Y. Chung, B. S. Mun, M. Salmeron and G. A. Somorjai, *Science*, 2008, **322**, 932.
20 B. Zugic, L. Wang, C. Heine, D. N. Zakharov, B. A. Lechner, E. A. Stach, J. Biener, M. Salmeron, R. J. Madix and C. M. Friend, *Nat. Mater.*, 2017, **16**, 558-564.
21 Z. Zhao, H. Liu, W. Gao, W. Xue, Z. Liu, J. Huang, X. Pan and Y. Huang, *J. Am. Chem. Soc.*, 2018, **140**, 9046-9050.
22 X. Shen, S. Dai, S. Zhang, Z. Lu, C. Zhang, G. W. Graham, Y. Lei, X. Pan and Z. Peng, *Chem. Mater.*, 2019, **31**, 1720-1728.
23 D. He, L. Zhang, D. He, G. Zhou, Y. Lin, Z. Deng, X. Hong, Y. Wu, C. Chen and Y. Li, *Nat. Commun.*, 2016, **7**, 12362.
24 Y. Zhao, J. Liu, C. Liu, F. Wang and Y. Song, *ACS Catal.*, 2016, **6**, 4127-4134.
25 Z. Nan, F. Yonggang, Z. Xing, G. Shaojun, G. Jun and H. Xiaoqing, *Adv. Mater.*, 2017, **29**, 1603774.
26 L. Bu, S. Guo, X. Zhang, X. Shen, D. Su, G. Lu, X. Zhu, J. Yao, J. Guo and X. Huang, *Nat. Commun.*, 2016, **7**.
27 J. Wang, F. Chen, Y. Jin and Y. Lei, *ACS Appl. Mater. Interfaces*, 2018, **10**, 6276-6287.
28 A. Wittstock, V. Zielasek, J. Biener, C. Friend and M. Bäumer, *Science*, 2010, **327**, 319-322.
29 G. G. Li, E. Villarreal, Q. Zhang, T. Zheng, J.-J. Zhu and H. Wang, *ACS Appl. Mater. Interfaces*, 2016, **8**, 23920-23931.
30 G.-T. Fu, C. Liu, Q. Zhang, Y. Chen and Y.-W. Tang, *Sci. Rep.*, 2015, **5**, 13703.
31 W. Liu, A.-K. Herrmann, N. C. Bigall, P. Rodriguez, D. Wen, M. Oezaslan, T. J. Schmidt, N. Gaponik and A. Eychmüller, *Acc. Chem. Res.*, 2015, **48**, 154-162.
32 B. Cai, D. Wen, W. Liu, A.-K. Herrmann, A. Benad and A. Eychmüller, *Angew. Chem. Int. Ed.*, 2015, **54**, 13101-13105.
33 D. Wen, A.-K. Herrmann, L. Borchardt, F. Simon, W. Liu, S. Kaskel and A. Eychmüller, *J. Am. Chem. Soc.*, 2014, **136**, 2727-2730.
34 C. Zhu, D. Wen, M. Oschatz, M. Holzschuh, W. Liu, A.-K. Herrmann, F. Simon, S. Kaskel and A. Eychmüller, *Small*, 2015, **11**, 1430-1434.
35 Q. Shi, C. Zhu, Y. Li, H. Xia, M. H. Engelhard, S. Fu, D. Du and Y. Lin, *Chem. Mater.*, 2016, **28**, 7928-7934.
36 J. Wang, F. Chen, Y. Jin and R. L. Johnston, *ChemSusChem*, 2018, **11**, 1354-1364.
37 W. Luo, X. Gao, S. Chou, J. Wang and H. Liu, *Adv. Mater.*, 2015, **27**, 6862-6869.
38 X. Gao, R. J. Esteves, T. T. H. Luong, R. Jaini and I. U. Arachchige, *J. Am. Chem. Soc.*, 2014, **136**, 7993-8002.
39 J.-H. Wang, W.-L. Dai, J.-F. Deng, X.-M. Wei, Y.-M. Cao and R.-S. Zhai, *Appl. Surf. Sci.*, 1998, **126**, 148-152.
40 F. Tao, M. E. Grass, Y. Zhang, D. R. Butcher, J. R. Renzas, Z. Liu, J. Y. Chung, B. S. Mun, M. Salmeron and G. A. Somorjai, *Science*,

View Article Online
DOI: 10.1039/C9NR03266E

2008, **322**, 932-934.
41 Y.-N. Wen and J.-M. Zhang, *Solid State Commun.*, 2007, **144**, 163-167.
42 A. Holewinski, J.-C. Idrobo and S. Linic, *Nat. Chem.*, 2014, **6**, 828-834.
43 Z. Xi, J. Li, D. Su, M. Muzzio, C. Yu, Q. Li and S. Sun, *J. Am. Chem. Soc.*, 2017, **139**, 15191-15196.
44 W. Huang, X. Ma, H. Wang, R. Feng, J. Zhou, P. N. Duchesne, P. Zhang, F. Chen, N. Han, F. Zhao, J. Zhou, W. Cai and Y. Li, *Adv. Mater.*, 2017, **29**, 1703057.
45 B. Cai, A. Dianat, R. Hubner, W. Liu, D. Wen, A. Benad, L. Sonntag, T. Gemming, G. Cuniberti and A. Eychmüller, *Adv. Mater.*, 2017, **29**, 1605254.
46 A. V. Tripković, K. D. Popović, B. N. Grgur, B. Blizanac, P. N. Ross and N. M. Marković, *Electrochim. Acta*, 2002, **47**, 3707-3714.
47 L. Ma, D. Chu and R. Chen, *Int. J. Hydrogen Energy*, 2012, **37**, 11185-11194.
48 D. A. Slanac, W. G. Hardin, K. P. Johnston and K. J. Stevenson, *J. Am. Chem. Soc.*, 2012, **134**, 9812-9819.
49 S. L. Horswell, A. L. N. Pinheiro, E. R. Savinova, M. Danckwerts, B. Pettinger, M.-S. Zei and G. Ertl, *Langmuir*, 2004, **20**, 10970-10981.
50 E. R. Savinova, A. Scheybal, M. Danckwerts, U. Wild, B. Pettinger, K. Doblhofer, R. Schlögl and G. Ertl, *Faraday Discuss.*, 2002, **121**, 181-198.
51 J. Zhang, M. Chen, H. Li, Y. Li, J. Ye, Z. Cao, M. Fang, Q. Kuang, J. Zheng and Z. Xie, *Nano Energy*, 2018, **44**, 127-134.

View Article Online
DOI: 10.1039/C9NR03266E

Table of Contents Entry:

An *in-situ* high-potential-driven restructuring of ternary AgPd-Pt$_{dilute}$ aerogels exhibits the unprecedented activity improvement for formate electrooxidation.